International Journal of Automotive Technology, Vol. 5, No. 1, pp. 47–53 (2004)

1229–9138/2004/015–06

CRUSH BEHAVIOR OF METALLIC FOAMS FOR PASSENGER CAR DESIGN

S. S. CHEON[1)*] and S. A. MEGUID[2)]

[1)]Division of Mechanical Engineering, Kongju National University, Chungnam 314-701, Korea
[2)]Engineering Mechanics and Design Laboratory, Department of Mechanical and Industrial Engineering, University of Toronto, 5 King's College Road, Toronto, Ontario, Canada M5S 3G8

(Received 7 August 2003; Revised 5 January 2004)

ABSTRACT–In this paper, a modified and representative unit cell model was employed to study the crush behaviour of a closed cell metallic foam. The unit cell which captures the main geometrical features of the metallic foam considered was used to simulate crush behaviour in metallic foams. Both analytical using limit analysis and numerical using the finite element method were used to study the collapse behaviour of the cell. The analytical crushing stress of the foam was compared with FE results and was found to be in good agreement.

KEY WORDS : Metallic foam, Crush behaviour, Plastic hinge analysis

1. INTRODUCTION

The improvement of the crashworthiness of automobiles cannot be overestimated. Also, environmental effects of vehicles are strongly considered nowadays (Mierlo *et al.*, 2003). This, together with a range of environmental concerns and social pressures backed by legislation has led, and will continue to lead, to highly innovative designs, involving lighter materials such as aluminium or magnesium alloys, smart structures, metal matrix and polymer matrix composites (Lee and Cheon, 2001), and metallic and polymeric foams. The use of these materials, however, is also governed by their ability to meet the increasing demands for crashworthiness (Huh and Kang, 2002) with the ultimate goal being the reduction of occupant harm and vehicle damage.

Of particular interest to this study is the use of structural foams in automotive components. Foam is currently being used as a filler material in bumpers and as reinforcement in roof and door beams. The objective is to reinforce these weak areas so that they respond effectively to impact loads. The energy absorbing capacity of foams is derived from their ability to undergo large deformation, while maintaining a near constant stress value.

Foam has been the subject of numerous experimental, numerical and theoretical investigations. Hanssen *et al.* (1996, 2000) studied foam filled structure analytically and experimentally. Baumeister *et al.* (1997) emphasized the integration of foam materials in the automotive body structure for energy absorption. Hučko and Faria (1997) used a simple viscoelastic material model to represent the mechanical behaviour of cellular materials. Sugimura *et al.* (1997) and Grenestedt (1998) assessed the roles of cell morphology and imperfections in governing the basic properties of foams, such as stiffness, yield strength and fracture resistance. Ford and Gibson (1998) developed microstructural models to examine the mechanisms responsible for differences in tensile and compressive strengths observed in cellular materials. Overaker *et al.* (1998) introduced a two-dimensional model for understanding the elastic behaviour of regular hexagonal foams as well as honeycomb structures. Santosa and Wierzbicki (1998, 1998) introduced a three-dimensional unit cell model and investigated the effect of key geometric parameters on the mechanical properties of the foam. Fortes *et al.* (1999) analyzed the contact of cellular solids based on a model previously developed by Gibson and Ashby (1988). Paul *et al.* (1999) performed experimental investigation on the tensile strength of notched closed cell aluminium foams. Harte *et al.* (1999) measured the tension-tension and compression-compression cyclic properties for aluminium foams. Miller (2000) proposed a yield surface that can be used to describe the plastic flow behaviour of metal foams. Deshpande and Fleck (2000) found that the dynamic behaviour of cellular aluminium alloys is very similar to their quasi-static behaviour up to a strain rate of 5000 s^{-1}. Batawros *et al.* (2000) and Meguid and Xue

*Corresponding author. e-mail: sscheon@kongju.ac.kr

(2000) experimentally investigated deformation mechanisms in a closed cell aluminium foams by digital image processing. Gutiérrez and Borst (2000) presented the application of the finite element reliability method to the evaluation of the statistical properties of localization phenomena. Meguid *et al.* (2002) introduced stochastic consideration to investigate localised deformation of cellular structures. The aim of the current work is to model the unit cell representing mechanical behaviour of cellular materials. Santosa and Wierzbicki's unit cell model (1998) used cruciform and pyramidal section, while it was deemed that pyramidal section is not good enough for the representative of cell shape. Therefore, the modification to Santosa and Wierzbicki's model is developed in this work using hemispherical as well as X section, which is believed to be more representative of the geometrical features of our foam and thermodynamically stabler, since hemispherical section is more representative compared with pyramidal section. The crush behaviour of the modified unit cell was studied analytically using plastic hinge analysis and compared with numerical simulation using the commercial FE code LS-DYNA.

2. MODIFIED UNIT CELL MODEL

Figure 1 shows the topology of closed cell aluminium foam fabricated by the Norsk Hydro.

Cell shapes are mostly spherical due to high surface tension prior to solidification. In this study, the pyramidal part of the cruciform-pyramid unit cell model of Santosa and Wierzbicki (1998) was replaced by a hemispherical section. As a result, the modified unit cell is composed of an X-section, upper and lower wings, a flat bottom and

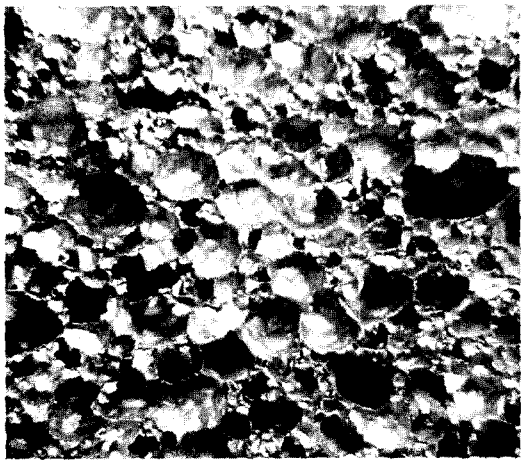

5 10 (mm)

Figure 1. Section of Hydro aluminium foam.

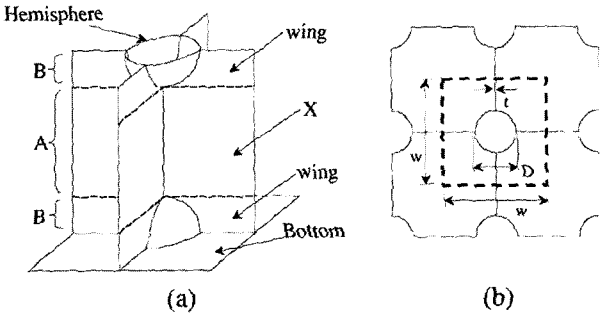

Figure 2. Modified unit cell model: (a) orthogonal view, and (b) oblique view.

two hemispherical parts, as depicted in Figures 2(a) and 2(b).

The relative density of the modified unit cell with respect to the solid cube can be expressed as

$$\frac{\rho_{foam}}{\rho_{solid}} = 3\left(\frac{t}{w}\right) + \frac{\pi}{4}\left(\frac{t}{w}\right)\left(\frac{D}{w}\right)^2 \tag{1}$$

The different components of the modified unit cell model absorb energy by membrane and bending deformations. It was assumed that the X-section and the wings only experience bending deformation. Furthermore, we assumed that the hemispherical part absorbs energy both by membrane and bending. Hereinafter, part A will imply the X-section, while part B implies the wings together with the hemispherical sections, as shown in Figure 2(b).

3. CRUSHING STRESS

Cellular materials undergo three steps of deformation during compressive loading: elastic, plateau and densification. The shock absorbing property of cellular structures depends on the plateau region. In this section, we evaluate the crushing stress of the modified unit cell model using plastic hinge analysis. The cell material was assumed to be elastic-perfectly plastic with a flow stress σ_F. The equivalent plastic flow stress (σ_F) for a general material behaviour can be obtained according to Schey (1987):

$$\sigma_F = \frac{1}{(\varepsilon_{pu} - \varepsilon_y)} \int_{\varepsilon_y}^{\varepsilon_{pu}} \sigma_p d\varepsilon_p \tag{2}$$

where, σ_p is the plastic stress, ε_p is the plastic strain, ε_{pu} is the ultimate plastic strain, and ε_y is the yield strain.

3.1. Mean Crushing Stress of Part A

The mean crushing stress of part A, i.e. σ_A was calculated based on the solution of Abramowicz (1994):

$$\sigma_A = \frac{P_A}{A_{bottom}} = 4.24\sigma_F\left(\frac{t}{w}\right)^{1.53} \tag{3}$$

3.2. Mean Crushing Stress of Part B

The mean crushing stress of the hemispherical part and the wings was evaluated using the energy equation:

$$P_B\delta_B = \sum_{i=1}^{n}\int \overline{M}_i l_i d\alpha + \int_S N_{\alpha\beta}\varepsilon_{\alpha\beta}dS \tag{4}$$

where P_B and δ_B imply mean crushing force and deformation of part B up to the onset of densification. $\overline{M}_i$ is the bending moment per unit length, l_i is the length on which $\overline{M}_i$ acts, i.e. the horizontal perimeter of the hemispherical part at an arbitrary polar angle and α is the rotated angle of the structure due to bending. The left hand side represents energy due to the external load and the right hand side contains the internal energy resulting from bending and membrane deformations. S is the surface experiencing membrane deformation.

In this hinge analysis, we assumed that the hemispherical part deforms plastically to form a circular disc upon densification, as shown in Figure 3. We can, therefore, calculate the height of the hemisphere at the onset of densification by assuming that negligible strain occurs in the polar direction ($\varepsilon_{\phi\phi}$) of the hemisphere prior to densification; viz.

$$h_d = \left(\frac{\pi}{4} - \frac{1}{2}\right)D \tag{5}$$

This implies that the onset of densification is dictated by membrane deformation not bending. Accordingly, the strain at the onset of densification can be determined as:

$$\varepsilon_d = \frac{w - 2h_d}{w} = 1 - 2\left(\frac{\pi}{4} - \frac{1}{2}\right)\frac{D}{w} = 1 - 0.6\frac{D}{w} \tag{6}$$

3.2.1. Energy due to bending in hemisphere

The bending deformation of the hemispherical part was divided into two stages. The first is a flattening stage, while the second involved the development of a hinge as shown in Figure 4.

Assuming that E_1 and E_2 denote the energy of the first and second stages, we can obtain

$$E_1 = \int_0^{\pi/2}\overline{M}l d\phi = \int_0^{\pi/2}\overline{M}_F(\pi D\sin\phi)d\phi$$
$$= (0.25\pi)\sigma_f Dt^2 = 0.8\sigma_F Dt^2 \tag{7a}$$

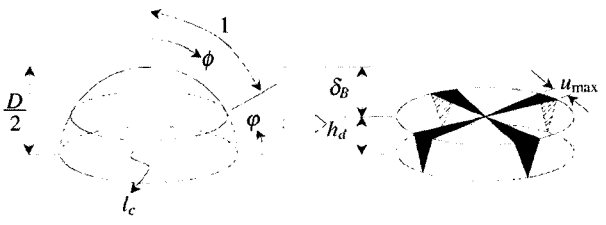

Figure 3. Membrance deformation of hemisphere.

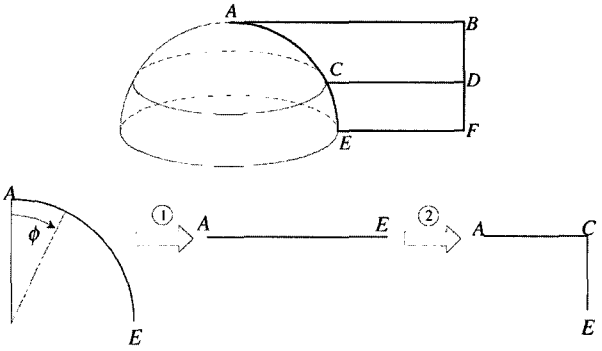

Figure 4. Bending deformation of hemisphere.

$$E_2 = \overline{M}_F l_c\frac{\pi}{2} = (0.25\sigma_F t^2)(\pi D\sin 1)\frac{\pi}{2}$$
$$= \frac{\pi^2}{8}(\sin 1)\sigma_F Dt^2 = \sigma_F Dt^2 \tag{7b}$$

where $\overline{M}_F$ is the bending moment per unit length corresponding to the flow stress, and l_c is the critical horizontal perimeter in the hemispherical part as shown in Figure 3. Their values are shown below

$$\overline{M}_F = 0.25\sigma_F t^2 \tag{8a}$$
$$l_c = \pi D\sin 1 = 2.6D \tag{8b}$$

Thus, the total energy due to bending in the hemisphere is

$$E_{hb} = E_1 + E_2 = 1.8\sigma_F Dt^2 \tag{9}$$

3.2.2. Energy due to membrane in hemisphere

The energy due to membrane deformation of the hemisphere E_m, based on the deformation mode shown in Figure 3, can be expressed in spherical coordinates, as follows:

$$\int_S N_{\alpha\beta}\varepsilon_{\alpha\beta}dS = \int_S (N_{rr}\varepsilon_{rr} + N_{\theta\theta}\varepsilon_{\theta\theta} + N_{\phi\phi}\varepsilon_{\phi\phi} + N_{r\theta}\varepsilon_{r\theta}$$
$$+ N_{\theta\phi}\varepsilon_{\theta\phi} + N_{r\phi}\varepsilon_{r\phi})dS \tag{10}$$

where θ is the azimuthal angle and ϕ is the polar angle. The above expression involves only one dominant membrane strain term ($\varepsilon_{\theta\theta}$). Since there is no deformation in the polar direction, $\varepsilon_{r\phi}$, $\varepsilon_{\phi\phi}$ and $\varepsilon_{\theta\phi}$ can be set to zero. Furthermore, the shear strains are negligible in membrane deformation, hence $\varepsilon_{r\theta}$ is also set to zero. The through-thickness strain ε_{rr} is not significant, and it is related to $\varepsilon_{\theta\theta}$ through Poisson's ratio. However, the radial stress resultant N_{rr} is negligible for thin structures. Based on these assumptions, Equation (10) becomes

$$\int_S N_{\alpha\beta}\varepsilon_{\alpha\beta}dS = \int_S N_{\theta\theta}\varepsilon_{\theta\theta}dS \tag{11}$$

where $N_{\theta\theta}$ and $\varepsilon_{\theta\theta}$ are given by

$$N_{\theta\theta} = \sigma_F t \tag{12a}$$

$$\varepsilon_{\theta\theta} = \frac{1}{r\sin\phi}\frac{\partial u_\theta}{\partial\theta} + \frac{u_r}{r} + \frac{u_\phi}{r}\cos\phi \tag{12b}$$

For membrane deformation, the angular displacement u_ϕ is equal to zero. In addition, the radial displacement u_r is accounted for in bending deformation. Accordingly, Equation (12b) can be expressed as

$$\varepsilon_{\theta\theta} = \frac{1}{r\sin\phi}\frac{\partial u_\theta}{\partial\theta} \tag{13}$$

Applying Equations (12a) and (13) to Equation (11), we obtain

$$\int_S (\sigma_F t)\left(\frac{1}{r\sin\phi}\frac{\partial u_\theta}{\partial\theta}\right)dS = \sigma_F t r\int\int\frac{1}{\sin\phi}\frac{\partial u_\theta}{\partial\theta}d\theta d\phi$$

$$= \sigma_F t\frac{D}{2}\int\frac{u_\theta}{\sin\phi}d\phi \tag{14}$$

where the maximum value of u_θ, i.e. $u_{\max}$, can be derived as follows:

$$u_{\max} = \frac{1}{4}(\pi D - \pi D\sin 1) = 0.1D \tag{15}$$

The polar displacement u_θ can be obtained as a function of ϕ and φ ($=\pi/2-\phi$), as well as u_{max} from the following geometric relations as shown in Figure 3.

$$u_\theta = u_{\max}\phi = 0.1D\phi \qquad (0 \le \phi \le 1) \tag{16a}$$

$$u_\theta = u_{\max}\frac{\varphi}{\left(\frac{\pi}{2}-1\right)} = 0.2D\varphi \qquad \left(0 \le \varphi \le \frac{\pi}{2}-1\right) \tag{16b}$$

Substituting Equation (16) into Equation (14), we obtain

$$\sigma_F t\frac{D}{2}\int\frac{u_\theta}{\sin\phi}d\phi$$

$$= \sigma_F t\frac{D}{2}\left[0.1D\int_0^1\frac{\phi}{\sin\phi}d\phi + 0.2D\int_0^{\frac{\pi}{2}-1}\frac{\varphi}{\sin\varphi}d\varphi\right] \tag{17}$$

The solution of this integration can be obtained using the following series expansion:

$$\int\frac{x\,dx}{\sin\alpha x}$$

$$= \frac{1}{\alpha^2}\left[\alpha x + \frac{(\alpha x)^3}{18} + \cdots + \frac{(2^{2n}-2)B_n(\alpha x)^{2n+1}}{(2n+1)!} + \cdots\right] \tag{18}$$

where B_n is Bernoulli number (Spiegel, 1968) defined as

$$B_n = \frac{(2n)!}{2^{2n-1}\pi^{2n}}\sum_{j=1}^{\infty}\frac{1}{j^{2n}} \tag{19}$$

The first three terms of the series solution of Equation (18) were considered sufficient resulting in a maximum error of 0.03% compared with numerical integration results using the trapezoidal rule. The total membrane energy absorbed by the hemispherical part is four times the contribution of Equation (17), i.e.,

$$E_{hm} = 4\left[\sigma_F t\frac{D}{2}\{(0.1D)(1) + (0.2D)(0.6)\}\right]$$

$$= 0.5\sigma_F D^2 t \tag{20}$$

3.2.3. Energy due to bending in wing

The energy due to bending in the wing sections can be obtained as follows. Let l denote the hinged length that undergoes folding, and α the rotating angle of the hinged section, with the help of Figure 4, then

$$E_{wb} = 4\bar{M}_F\sum l_i\alpha_i$$

$$= \bar{M}_F[l_{AB}\alpha_{AB} + 2l_{CD}\alpha_{CD} + l_{EF}\alpha_{EF} + l_{ACE}\alpha_{ACE}]$$

$$= 4\bar{M}_F\left[\frac{w}{2}\frac{\pi}{2} + 2\left(\frac{w}{2}-\frac{w}{2}\sin 1\right)\frac{\pi}{2} + \left(\frac{w}{2}-\frac{D}{2}\right)\frac{\pi}{2} + \frac{\pi D}{4}\frac{\pi}{2}\right]$$

$$= (3.1w - 0.9D)\sigma_F t^2 \tag{21}$$

3.2.4. Crushing stress

The total displacement of part B, δ_B (Figure 3) can be expressed as

$$\delta_B = \frac{D}{2} - h_d = 0.2D \tag{22}$$

Applying Equations (9), (20), (21) and (22) to Equation (4), and isolating P_B results in

$$P_B = \frac{1}{0.2D}[(3.1w-0.9D)\sigma_F t^2 + 1.8\sigma_F D t^2 + 0.5\sigma_F D^2 t]$$

$$= \sigma_F\left(14.6\frac{w}{D}t^2 + 4.4t^2 + 2.4Dt\right) \tag{23}$$

The mean crushing stress of part B can therefore be expressed as:

$$\sigma_B = \frac{P_B}{A_{bottom}}$$

$$= 14.6\sigma_F\left(\frac{t}{D}\right)\left(\frac{t}{w}\right) + 4.4\sigma_F\left(\frac{t}{w}\right)^2 + 2.4\sigma_F\left(\frac{D}{w}\right)\left(\frac{t}{w}\right) \tag{24}$$

3.3. Total Crushing Stress

The total displacement of part A, δ_A can be expressed as

$$\delta_A = w - 2h_d = w - 0.6D \tag{25}$$

The total crushing stress of the modified unit cell model can be obtained by taking the average crushing stress of each part with respect to vertical deformation, such that:

$$\sigma_T = \frac{\sum \sigma_j \delta_j}{\sum \delta_j} = \frac{\sigma_A \delta_A + 2\sigma_B \delta_B}{\delta_A + 2\delta_B}$$
$$= \frac{\sigma_A(w - 0.6D) + 2\sigma_B(0.2D)}{(w - 0.6D) + 2(0.2D)}$$
$$= \frac{\sigma_A(w - 0.6D) + 0.4\sigma_B D}{w - 0.2D} \quad (26)$$

where σ_A and σ_B, the crushing stresses of parts A and B were given in Equations. (3) and (24), respectively. The effect of density on the total crushing stress is compared with numerical results in the next session (Santosa and Wierzbicki, 1998).

4. NUMERICAL CHARACTERISATION

The crushing results of modified unit cell models were compared with finite element simulations using LS-DYNA. Four-noded shell elements were used for the unit cell and three-noded shell elements were introduced for connecting between the wing and hemisphere sections. A total of 2200 shell elements were used for the unit cell. The Belytschko-Tsay shell element with reduced integration, hourglass control and self contact were considered. A piecewise linear plastic material model was used for the unit cell material with AA6063-T7 material properties. Tables 1 and 2 show the material properties that were used for the modified unit cell model and the loading platen. Automatic surface-to-surface contact was invoked between the model and the platens. Transverse shear effects were automatically considered. The unit cell model was compressed at a speed of 200 mm/sec. In the present study, a diameter to width ratio of 0.5 was selected. According to Equation (6), this yields a 70% densification strain, which is in agreement with preliminary compressive test results of aluminium foams. Finite

Table 1. Material properties used in FE analyses.

	Cell	Rigid platen
Density	2770 kg/m^3	7800 kg/m^3
Elastic modulus	69 GPa	200 GPa
Yield stress	87 MPa	Not necessary
Poissons ratio	0.3	0.33

Table 2. Plastic stress-plastic strain relations used for Aluminium foam cell (Santosa and Wierzbicki, 1998).

Plastic strain (%)	Plastic stress (MPa)
0	87
0.03	96
0.2	100
0.6	110
1.5	130
2.5	140
7	170
15	171

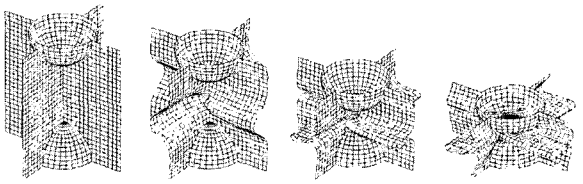

Figure 5. Deformation of the modified unit cell model at different strain levels: (a) 0.1%, (b) 25%, (c) 50%, and (d) 70%.

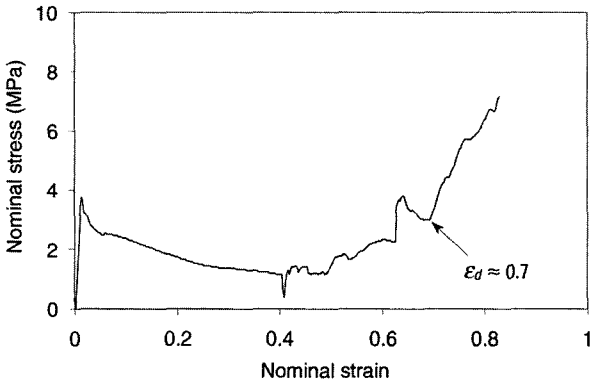

Figure 6. Stress-strain curve for 6.5% relative density foam based on modified unit cell model.

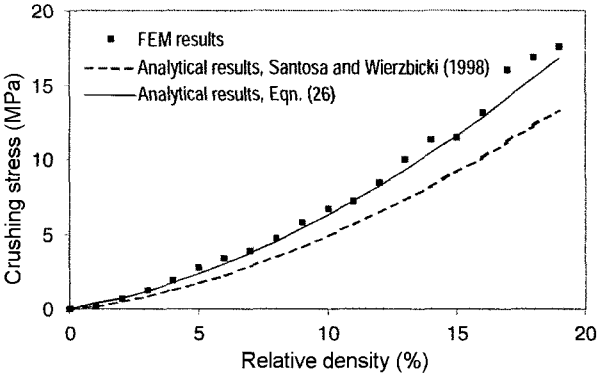

Figure 7. Variation of crushing stress with relative foam density.

element analyses were performed for different relative density ratios by changing the cell wall thickness to width ratio. Figure 5 depicts the deformation of the modified unit cell model and Figure 6 shows the nominal stress-nominal strain curves for a relative foam density of 6.5%. The conspicuous cusp, occurring at 41% strain, can be attributed to the snap-through buckling of the hemispherical part.

The numerically predicted densification strain is in agreement with the analytical result of Equation (6). The plastic flow stress (σ_F) of the material for the plastic hinge analysis was assumed to be 160 MPa according to Equation (2).

Figure 7 shows a comparison between the analytical crushing stress of Equation (26) and that of Santosa and Wierzbickis pyramid-cruciform (1998) with the finite element predictions for different relative foam densities. The finite element results are in good agreement with Equation (26), while Santosa and Wierzbicki's model underestimates the crushing stresses.

5. CONCLUSIONS

A modified unit cell model was developed using hemispherical as well as X-section, which is believed to be more representative of the geometrical features of aluminium foam and thermodynamically stabler, and employed in the analysis of the crushing behaviour of metallic foams with plastic hinge analyses. The verification of the modified unit cell model was carried out using FE analyses. In this respect, a plastic hinge analysis of the collapse behaviour of the unit cell was compared with finite element predictions and the results were found to be in good agreement. Moreover, the modified unit cell model showed better results than Santosa and Wierzbicki's model.

ACKNOWLEDGEMENT–This work was financially supported by KISTEP (Korea Institute of Science and Technology Evaluation and Planning) with grant number of M102DB010002-03D0201-00213.

REFERENCES

Abramowicz, W. (1994). Crush resistance of T, Y, and X sections. *Technical Report 24*, Department of Ocean Engineering, MIT, Cambridge, MA-02139, U.S.A.

Bastawros, A-F., Bart-smith, H. and Evans, A. G. (2000). Experimental analysis of deformation mechanisms in a closed-cell aluminium alloy foam. *J. the Mechanics and Physics of Solids*, **48**, 301–322.

Baumeister, J., Banhart, J. and Weber, M. (1997). Aluminium foams for transport industry. *Materials & Design*, **18**, 217–220.

Deshpande, V. S. and Fleck, N. A. (2000). High strain rate compressive behaviour of aluminium alloy foams. *Int. J. Impact Engineering*, **24**, 277–298.

Ford, C. M. and Gibson, L. J. (1998). uniaxial strength asymmetry in cellular materials: An analytical model. *Int. J. Mechanical Science*, **40**, 521–31.

Fortes, M. A., Colaço, R. and Vaz, M. F. (1999). The contact mechanics of cellular solids. *Wear*, **99**, 2301–2310.

Gibson, L. J. and Ashby, M. F. (1998). *Cellular Solids*. Pergamon Press. Oxford, England.

Grenestedt, J. L. (1998). Influence of wavy imperfections in cell walls on elastic stiffness of cellular solids. *J. the Mechanics and Physics of Solids*, **45**, 29–50.

Gutiérrez, M. A. and Borst, R. D. (2000). Stochastic aspects of localized failure: material and boundary imperfections. *Int. J. Solids and Structures*, **37**, 7145–7159.

Hanssen, A. G., Langseth, M. and Hopperstad, O. S. (1996). Static crushing of square aluminium extrusions with aluminium foam filler. *Int. J. Impact Engineering*, **18**, 949–968.

Hanssen, A. G., Langseth, M. and Hopperstad, O. S. (2000). Static and dynamic crushing of square aluminium extrusions with aluminium foam filler. *Int. J. Impact Engineering*, **24**, 347–383.

Harte, A. M., Fleck, N. A. and Ashby, M. F. (1999). Fatigue failure of an open cell and a closed cell aluminium alloy foam. *Acta Materialia*, **47**, 2511–2524.

Hučko, B. and Faria, L. (1997). Material model of metallic cellular solids. *Computers & Structures*, **62**, 1049–1057.

Huh, H. and Kang, W. J. (2002). Crash-worthiness assessment of thin-walled structures with the high-strength steel sheet. *Int. J. Vehicle Design*, **30**, 1–21.

Lee, D. G. and Cheon, S. S. (2001). Impact characteristics of glass fiber composites with respect to fiber volume fraction. *J. of Composite Materials*, **35**, 27–56.

Meguid, S. A., Cheon, S. S. and Abbasi, N-El (2002). FE modelling of deformation localization in metallic foams. *Finite Elements in Analysis and Design*, **38**, 631–643.

Meguid, S. A. and Xue, H. (2000). On the use of "SDDIS" for measuring deformation localization in cellular materials. *Proceedings of the third International Conference on Mechanics and Materials in Design*. Orlando, U.S.A. 187.

Mierlo, J. V., Vereecken, L., Maggetto, G., Favrel, V., Meyer, S. and Hecq, W. (2003). How to define clean vehicles? Environmental impact rating of vehicles. *Int. J. Automotive Technology*, **4, 2**, 77–86.

Miller, R. E. (2000). A continuum plasticity model for the constitutive and indentation behaviour of foamed

metals. *Int. J. Mechanical Science*, **42**, 729–754.

Overaker, D. W., Cuitiño, A. M. and Langrana, N. A. (1998). Effects of morphology and orientation on the behavior of two-dimensional hexagonal foams and application in a re-entrant foam anchor model. *Mechanics of Materials*, **29**, 43–52.

Paul, A., Seshacharyulu, T. and Ramanurty, U. (1999). Tensile strength of a closed-cell al foam in the presence of notches and holes. *Scripta Materialia*, 40, 809–814.

Santosa, S. and Wierzbicki, T. (1998). Crash behavior of columns filled with aluminum honeycomb or foam. *Computers and Structures*, **68**, 343–367.

Santosa, S. and Wierzbicki, T. (1998). On the modeling of crush behavior of a closed-cell aluminium foam structures. *J. the Mechanics and Physics of Solids*, **46**, 645–669.

Schey, J. A. (1987) *Introduction to Manufacturing Processes*. McGraw-Hill. New York.

Spiegel, M. R. (1968). *Mathematical Handbook of Formulas and Tables*. McGraw-Hill. New York.

Sugimura, Y., Meyer, J., He, M. Y., Bart-smith, H., Grenestedt, J. L. and Evans A G. (1997). On the mechanical performance of closed cell al alloy foams. *Acta Materialia*, **45**, 5245–5259.